Phase transitions and phonon thermodynamics in giant piezoelectric Mn-doped K$_{0.5}$Na$_{0.5}$NbO$_3$-LiBiO$_3$ crystals studied by Raman spectroscopy

Anyang Cui (崔安阳),[1] Xihua Cao (曹锡华),[1] Yan Ye (叶艳),[1] Kai Jiang (姜凯) ⓞ,[1] Liangqing Zhu (朱亮清),[1]
Minhong Jiang (江民红),[2,*] Guanghui Rao (饶光辉),[2] Yawei Li (李亚巍),[1]
Zhigao Hu (胡志高),[1,3,4,†] and Junhao Chu (褚君浩)[1,3,4]

[1]*Technical Center for Multifunctional Magneto-Optical Spectroscopy (Shanghai),*
Engineering Research Center of Nanophotonics Advanced Instrument (Ministry of Education), Department of Materials,
School of Physics and Electronic Science, East China Normal University, Shanghai 200241, China
[2]*Guangxi Key Laboratory of Information Materials, School of Materials Science and Engineering,*
Guilin University of Electronic Technology, 541004, Guilin, Guangxi, China
[3]*Collaborative Innovation Center of Extreme Optics, Shanxi University, Taiyuan, Shanxi 030006, China*
[4]*Shanghai Institute of Intelligent Electronics & Systems, Fudan University, Shanghai 200433, China*

Ferroelectric lead-free K$_x$Na$_{1-x}$NbO$_3$ (KNN) perovskite, as the representative of the preferred oxides with good dielectric and piezoelectric behaviors, has attracted broad attentions in recent years. Here we systematically investigate the complete process of temperature dependent structural evolution in manganese (Mn)-doped K$_{0.5}$Na$_{0.5}$NbO$_3$-LiBiO$_3$ single crystals, presenting the ultrahigh piezoelectric coefficient of about 1050 pC N^{-1} and the excellent dielectric and ferroelectric performances, by demonstrating phonon thermodynamics associated with all Raman active modes at a wide temperature range of 80–800 K. All-round unpolarized and polarized scattering characteristics reflecting various phonon and structure properties are specified in detail. Symmetry difference, symmetry breaking, and structure rearrangement among the molecular vibrations have been proven to be related to a multiphase coexistence and the discontinuity of first-order phase transition. In comparison with the lattice dynamics, a complete phase transition ordering and the shift of transition point have been observed in KNN-LiBiO$_3$ crystals with the different Mn contents. This work aims at deeply revealing the details of good ferroelectric/dielectric performance, structure, and phonon thermodynamics, as well as understanding the mechanisms of first-order phase transition under the doping manipulation in KNN systems.

I. INTRODUCTION

Potassium sodium niobate K$_x$Na$_{1-x}$NbO$_3$ (KNN) is of increasingly great concern depending on its excellent piezoelectric coefficient (d_{33}) [1], after the Restriction of Hazardous Substances (RoHS) released by the European Union demanded a reduction in the use of lead element. Conventionally, Pb(Zr, Ti)O$_3$ (PZT) is widely used due to high piezoelectric behavior and almost the vertical separation between the rhombohedral and the tetragonal state [2]. In order to develop environment-friendly KNN-based materials and applications instead of PZT products, much attention has been paid in recent years to improve the piezoelectric performance of KNN by modifying the doping and synthesis methods [1,3–6]. However, fewer studies focus on exploring the details of phase transition and its underlying mechanism. Investigating phase properties and lattice evolution in view of condensed matter is fundamentally important for developing the performance and applications of KNN-based crystals [7]. Therefore, more specific studies on the structural behavior of KNN-series ferroelectrics are worth carrying out, such as effects of the crystalline quality (i.e., leakage current) and the doping on ferroelectric ordering phase transition.

For pure KNN ($x = 0.5$), phase transition from rhombohedral (R) to orthorhombic (O) is located at approximately 170 K, from orthorhombic (O) to tetragonal (T) transition at near 493 K, and tetragonal (T) to cubic (C) transition at near 693 K (Curie temperature T_c), respectively [8]. To obtain the excellent piezoelectric performances, different doping schemes have been attempted in KNN series, such as the substitutions of Mn, Li, Ta, Sb, Bi, or Zr ions in A site or B site of the oxygen octahedra (ABO$_3$) structure [4,9–14]. Among these modified doping substances, manganese (Mn) ion acts as a popular and interesting additive. The Mn ion could possibly substitute A or B sites as electron or hole absorbent [15], thus efficiently contributing to improve space charge polarization behaviors, as well as the great reduction of leakage current by about two orders of magnitude [16,17]. However, investigating the effect of the varied doping and its content on structure and phase transition is still absent, in terms of deep physical comprehension by effective spectroscopic approaches.

As one of molecular vibration spectroscopy techniques, Raman scattering is competent for investigating the internal strain, crystallinity, chemical-bond property,

molecular polarizability, and symmetry of ferroelectrics [18–22]. The scattering signal performs at high sensitivity on perceiving the tiny distortion of lattice during the structural (ferroelectric-paraelectric ordering) or nonstructural (ferromagnetic-paramagnetic ordering) phase transitions [23–25]. Structure phase transition of crystal generally leads to an anomalous shift of phonon frequency, which could be distinguished from the phonon-occupation-driven and volume-dilatation-driven contributions [26]. Instead of the common scattering criteria of phonon frequency and linewidth, especially, previous studies in both theory and experiment have confirmed that the polarized Raman scattering intensity and depolarization ratio from scattering in double cross-polarized geometries perform unique functionality on determining first-order phase transition, lattice symmetry, and molecular vibration geometry [26–31].

In this study, the crystal matrices of 0.25% Mn-doped $0.996K_{0.5}Na_{0.5}NbO_3$-$0.004LiBiO_3$ (KNNLB-25Mn) and 0.375% Mn-doped $0.996K_{0.5}Na_{0.5}NbO_3$-$0.004LiBiO_3$ (KNNLB-37Mn) solid solutions are prepared with the great-optimized ferroelectric, piezoelectric, and dielectric performances. Complete temperature dependent phase transitions of them are systematically investigated by Raman spectroscopy at 80–800 K. Our previous report [17] has presented the ultrahigh and stable piezoelectric coefficient d_{33} of about 1050 pC N^{-1} and a high remnant polarization P_r of 40 $\mu C\,cm^{-2}$ in KNNLB-37Mn single crystal. Theoretically, the ferroelectric KNN single crystal embraces better piezoelectric response, the optimal crystallographic orientation, and the controllable polarization engineering than a polycrystalline solid solution [17,32]. Scattering characteristics of the phonon frequency, linewidth, polarized scattering intensity, and depolarization ratio are collected and systematically analyzed using the polarized and unpolarized scattering geometries, accompanied by phase transition in first-order process [20,26,33,34]. Notably, the physical correlations between a perovskite-typed ferroelectric molecule and the scattering signals have been systematically discussed. Thermal kinetics of NbO_6 octahedra also exhibit some distinct changes and phase coexistence near the transformation boundary by exploring phonon characteristics under the thermal control. It indicates an entire phase transition process in the KNNLB system corresponding to a full phase ordering: R to O to T to C phase transition ordering. This work would provide some primary evidences for understanding the physical correlation between the unique structure characteristics and the excellent functionality in KNN-based crystals.

II. MATERIALS AND METHODS

KNN based ferroelectric single crystals are synthesized mainly by the melt growth processes including floating zone method (FZM) [35], the flux-Bridgman method [20,36], top-seeded solution growth (TSSG) method [37], and so on. Here KNNLB-25Mn and KNNLB-37Mn single crystals were synthesized by a unique method of the seed-free, solid-state crystal growth (SFSSCG) method [17,38,39]. High-purity powders of Nb_2O_5 (99.5%), K_2CO_3 (99%), Na_2CO_3 (99.8%), Li_2CO_3 (97%), Bi_2O_3 (99%), and MnO_2 (85%) were employed as the raw reagents. After baking these powders at

200 °C and then weighing them, raw powders were mixed in ethanol by ball milling for 1 day. Then calcining the powders in air at 750 °C for 6 h. The dried materials need the ball-milling process again for 8 h before being pressed into pellets under the uniaxial pressure of over 90 MPa. The pressed products in pellets were sintered in air at a peak temperature of around 1090 °C for 18–21 h. As-grown doped KNN single crystal was carefully collected from the mixed crystal, oriented, polished, and mechanically cut. For exploring lattice structural characteristics by Raman scattering spectroscopy, the achieved single crystals were annealed for 10 h in air at 800 °C. KNNLB single crystals with different Mn contents were prepared successfully with a final thickness of about 0.6–0.8 mm, and a size of 2–4 mm in diameter. SFSSCG technique would effectively overcome the shortcomings of traditional melt growth methods on synthesizing ferroelectric oxides with complex compositions, such as the incongruent melting-induced composition inhomogeneity, high-temperature, and long-time process-induced volatility for Na_2O and K_2O species [16,35,38]. Seed-free method also eliminates the strong effect of the seed crystal on the quality of the prepared single crystal. Compositional homogeneity and good crystallinity have been confirmed on KNNLB and Mn-doped single crystals from SFSSCG methods by a number of experimental characterizations such as x-ray diffraction, scanning/transmission electron microscopy, energy dispersive spectrometer, and the basic chemical analysis, etc. in our previous work [17,38,39].

Raman spectroscopic measurements were performed on a Jobin-Yvon LabRAM HR Evolution micro-Raman spectrometer equipped with a Linkam THMSE 600 heating/cooling stage with a heating/cooling rate of 5 K/min and a temperature accuracy of ±0.1 K. Resolution of the spectrum is controlled as 1 cm^{-1}. The wavelength of excitation laser is 532 nm. To obtain the polarized scattering, the polarizers were placed in the excitation and detection path to define the parallel-polarized (VV) and the cross-polarized (VH) scattering configurations. Whole spectra were corrected for the Bose-Einstein thermal factor $n(\omega, T) = [\exp(\hbar\omega/kT) - 1]^{-1}$, where n is the reduced Raman data for the Bose-Einstein thermal factor, and $\hbar$, ω, k, and T are the reduced Planck constant, phonon wave number, Boltzmann constant, and temperature, respectively. The heat effect from laser beam can be ignored, owing to the power of less than 5 mV on samples. Ferroelectric polarization-electric field (P-E) hysteresis loops at room temperature were acquired at 10 Hz, using a ferroelectric test system (P-PMF, Radiant). Temperature dependence of dielectric constant and dielectric loss (tan δ) at a temperature range of 300–700 K were carried out at 10 and 100 kHz by employing an impedance analyzer (Agilent 4294A).

III. RESULTS AND DISCUSSION

Large-size KNN-LiBiO$_3$ crystal matrices with Mn cation doping have been prepared by a rapid and inexpensive crystal synthesis (SFSSCG) method. As a sintering aid, LiBiO$_3$ compounds with a low content contribute to the exaggerated grains in the single crystal matrix. Bismuth oxide added into KNN solutions with an appropriate addition would facilitate transportation, solution dissolution, and be beneficial to the crystal
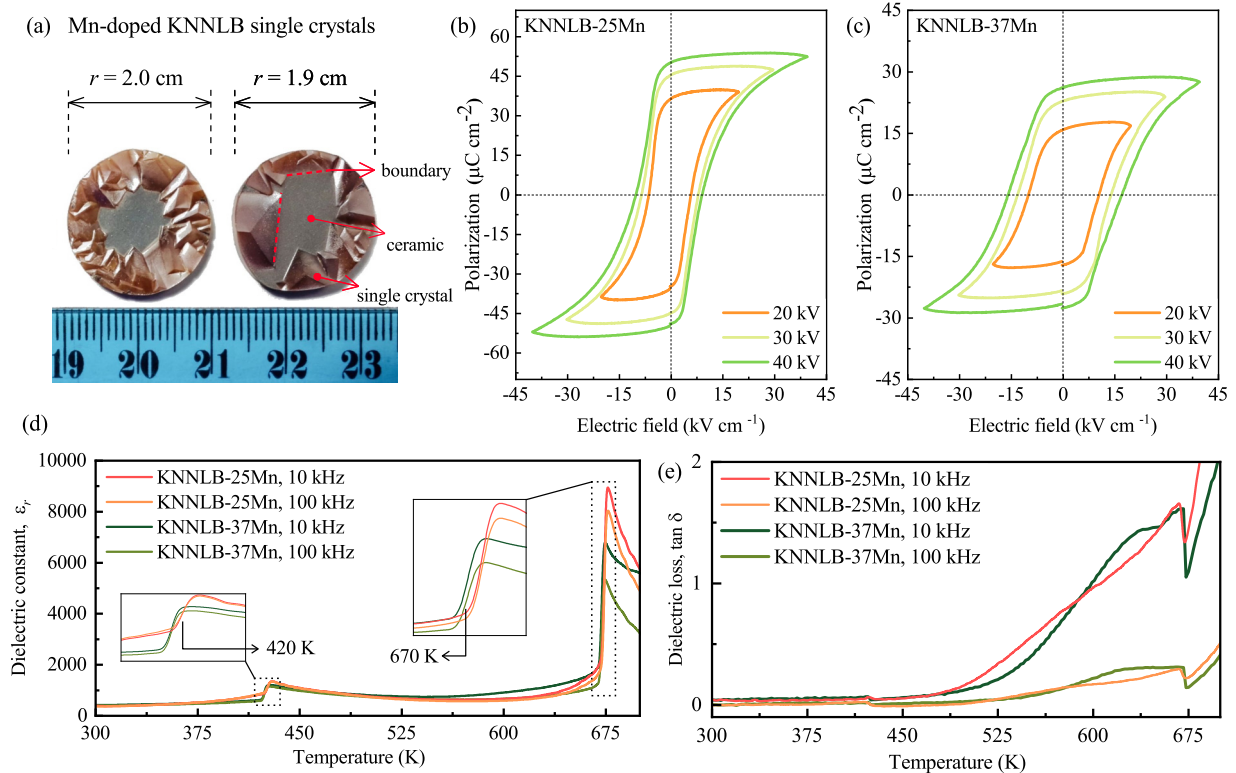
FIG. 1. (a) Photographs of the as-grown Mn-doped KNNLB crystal matrix, consisting of the exaggerated grain as the single crystal and polycrystalline ceramic areas. (b) and (c) Ferroelectric P-E loops at room temperature of KNNLB-25Mn and KNNLB-37Mn obtained at the electric field from -40 to $+40$ kV cm^{-1}, respectively. Temperature dependence (300–700 K) of (d) the dielectric permittivity and (e) the dielectric loss at 10 and 100 kHz for the varied doping KNNLB crystals, respectively. The enlarged areas in (d) highlight the sharp changes with increasing temperature.

growth rates [38]. The slight doping substance of MnO$_2$ does not affect the synthesis habit of KNN crystal by the SFSSCG technique. Figure 1(a) shows the photographs of the as-grown Mn-doped KNNLB samples, showing a coexistence state of the exaggerated grain and polycrystalline ceramic matrix regions. Well-defined boundaries are observed between the big single crystalline grains and the ceramic matrix. Note that the Mn-doped KNNLB single crystal grows from the edge toward the center [38]. Owing to the additional Mn substitution, the KNNLB single crystal matrix would present its homogeneous color of deep brown, where the size of the Mn-doped KNNLB sample is around 1.9 and 2.0 cm in diameter. Removing the polycrystalline matrix, the Mn-doped KNNLB single crystal then can be extracted by cutting and polishing the as-grown crystal matrix into a pellet for the following investigations of dielectric, ferroelectric properties, and crystalline structure characterizations by Raman scattering. Chemical analysis of samples by an energy dispersive spectrometer (EDS) has been carried out. EDS mapping results (not shown here) provide the basic evidence on the homogeneous chemical distribution of Mn cations in KNNLB single crystals, and the different content of Mn dopants for both samples.

Figures 1(b) and 1(c) demonstrate ferroelectric polarization characteristics with respect to the external electric field of -40 to $+40$ kV cm^{-1} at room temperature (25 °C) as P-E hysteresis loops on the unannealed KNNLB-37Mn and the unannealed KNNLB-25Mn crystals, respectively. The remnant polarization (P_r) of the 0.25% Mn-doped KNNLB crystals is about 50 μC cm^{-2}, and its coercive field (E_c) is approximately 10 kV cm^{-1}. Meanwhile, the P_r of the unannealed KNNLB-37Mn crystal is about 26 μC cm^{-2}, and its coercive field (E_c) is about 16 kV cm^{-1}. According to our previous report [17], it is noted that the annealing process during preparation of KNNLB-37Mn crystal would greatly improve its ferroelectric property, making P_r increase to about 40 μC cm^{-2} and E_c decline to 8 kV cm^{-1}. This enhanced ferroelectric performance after the thermal annealing process in air or O$_2$ atmosphere might be attributed to the improvement of the crystallization, which promoted the degree of the A-site or B-site spatial ordering in Mn-doped KNNLB crystals in order to minimize the total internal energy of the lattice, as well as suppressing the increased hole by the oxidation of these crystals [40]. Besides, the saturated loop in polarization state with a high P_r value reflects that Mn cation additives would positively contribute to reducing leakage current density and further improving ferroelectric response of KNN based crystals. Therefore, the structure exploration based on systematical experiments of Raman scattering around the main work in this paper is carried out on KNNLB single crystals after an annealing process in air for 10 h at 800 °C, depending on their excellent ferroelectric and dielectric properties under this circumstance.

Furthermore, the temperature dependent dielectric constant [$\varepsilon_r(T)$] and dielectric loss (tanδ) of KNNLB-25Mn and
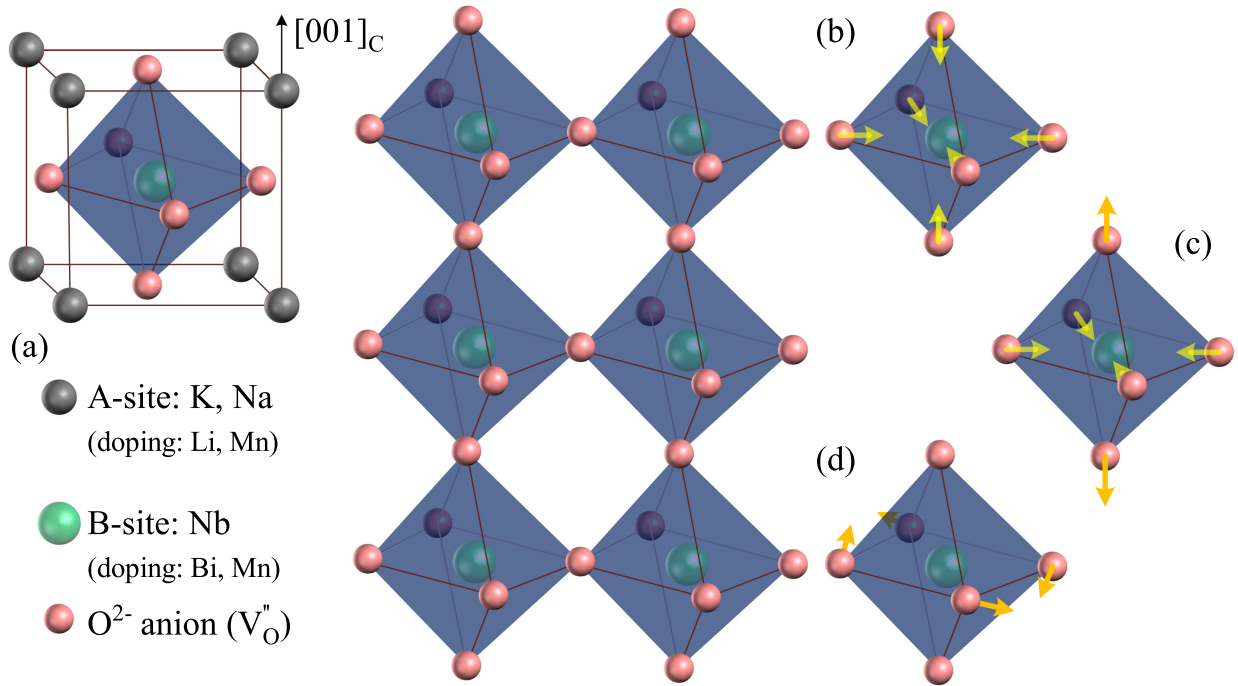
FIG. 2. Schematic diagrams showing (a) the pseudocubic lattice structure along the $[001]_C$ direction of the Mn cation doping KNNLB crystal, as well as its main internal vibrations of the oxygen octahedra: (b) The stretching $A_{1g}(\upsilon_1)$ mode, (c) the stretching $E_g(\upsilon_2)$ mode, and (d) the bending $F_{2g}(\upsilon_5)$ mode. As marked in (a), the main atoms at A and B sites are K, Na, and Nb, respectively, as well as the possible substitutions.

KNNLB-37Mn crystals in the range of 300–700 K have been implemented at 10 and 100 kHz, as depicted in Figs. 1(d) and 1(e). These results of temperature dependence can be used to clearly discuss the transitions of ferroelectric structure. We highlight the anomalous changes in the $\varepsilon_r(T)$ curves as two enlarged regions near 420 and 670 K in the insets of Fig. 1(d). Similar phenomena can be seen in temperature dependent $\tan\delta$ from KNNLB-25Mn and KNNLB-37Mn crystals. It is associated with the structural O-T and T-C phase transitions with the temperature increases, respectively. Particularly, it obviously shows that both O-T and T-C phase transition temperatures for KNNLB-37Mn shift a little toward room temperature in comparison with those for KNNLB-25Mn. The reduction of the transition point could be attributed to the Mn doping effect in KNN-LiBiO$_3$ perovskite. Moreover, the doping is generally considered to contribute to improve the multiphase coexistence near the phase transition boundary. Hence, we further implement temperature dependence of Raman scattering on both KNNLB crystals in order to carefully study their structure properties, such as phase transition ordering, multiphase coexistence, molecular symmetry, and phonon characteristics with the thermal-induced behaviors.

Both KNN and LiBiO$_3$ crystals possess the ABO$_3$ perovskite structure. KNNLB single crystals present the pure orthorhombic phase at room temperature confirmed by the x-ray diffraction results [17]. Figure 2(a) illustrates the pseudocubic lattice along the $[001]_C$ direction of Mn-doped KNNLB crystal. LiBiO$_3$ compound as one of the bismuthates contains Bi^{5+} with a $6s$ empty orbital, and hold the pure orthorhombic structure at room temperature following space group $Pccn$ and local symmetry D_{2h}^{10} [41]. Group theory

predicts basically that space group $Amm2$ (C_{2v}^{14}) of the undoped KNN lattice at room temperature presents pure orthorhombic phase with Raman-active optical modes of $4A_1 + 4B_1 + 3B_2 + A_2$. Entire vibrational configurations can be considered as the translational modes of cations (Li$^+$, Na$^+$, K$^+$) located mainly at lower than 200 cm^{-1} in Raman spectrum, and internal ones of BO$_6$ octahedra at the range of 200–900 cm^{-1} [3,26,42,43]. Specifically, the BO$_6$ octahedra consisting of six vibrations corresponds to $A_{1g}(\upsilon_1)$, $E_g(\upsilon_2)$, $F_{1u}(\upsilon_3)$, $F_{1u}(\upsilon_4)$, $F_{2g}(\upsilon_5)$, and $F_{2u}(\upsilon_6)$. Among these modes, $A_{1g}(\upsilon_1)$, $E_g(\upsilon_2)$, and $F_{1u}(\upsilon_3)$ meet stretching geometry, and the others are the bending ones. Figures 2(b)–2(d) depict the schematic representations of $A_{1g}(\upsilon_1)$, $E_g(\upsilon_2)$, and $F_{2g}(\upsilon_5)$ modes, which are the key three vibration behaviors of BO$_6$ octahedra and highly sensitive to be observed by Raman scattering spectrum.

It is generally accepted that phase structure determination of the K$_{0.5}$Na$_{0.5}$NbO$_3$ based ferroelectric system follows a complete R-O-T-C phase transition ordering with increasing temperature [8,44]. In detail, the basic units of both ferroelectric KNbO$_3$ and antiferroelectric NaNbO$_3$ at room temperature hold O phase [45,46]. A small quantity of K$^+$ composition is sufficient to change the initial structure of NaNbO$_3$ toward that of KNbO$_3$, where K$^+$ ion is relatively large in radius enough to fill the 12-coordinated cavity of the perovskite unit. The phase transition temperatures ($T_{R\text{-}O}$, $T_{O\text{-}T}$, and T_C) of the modified KNN crystal would be shifted by chemical substitutions [8,47].

In terms of recognizing phonon modes with their thermodynamics of Mn-doped KNNLB single crystals, phonon frequency is always regarded as the first parameter to
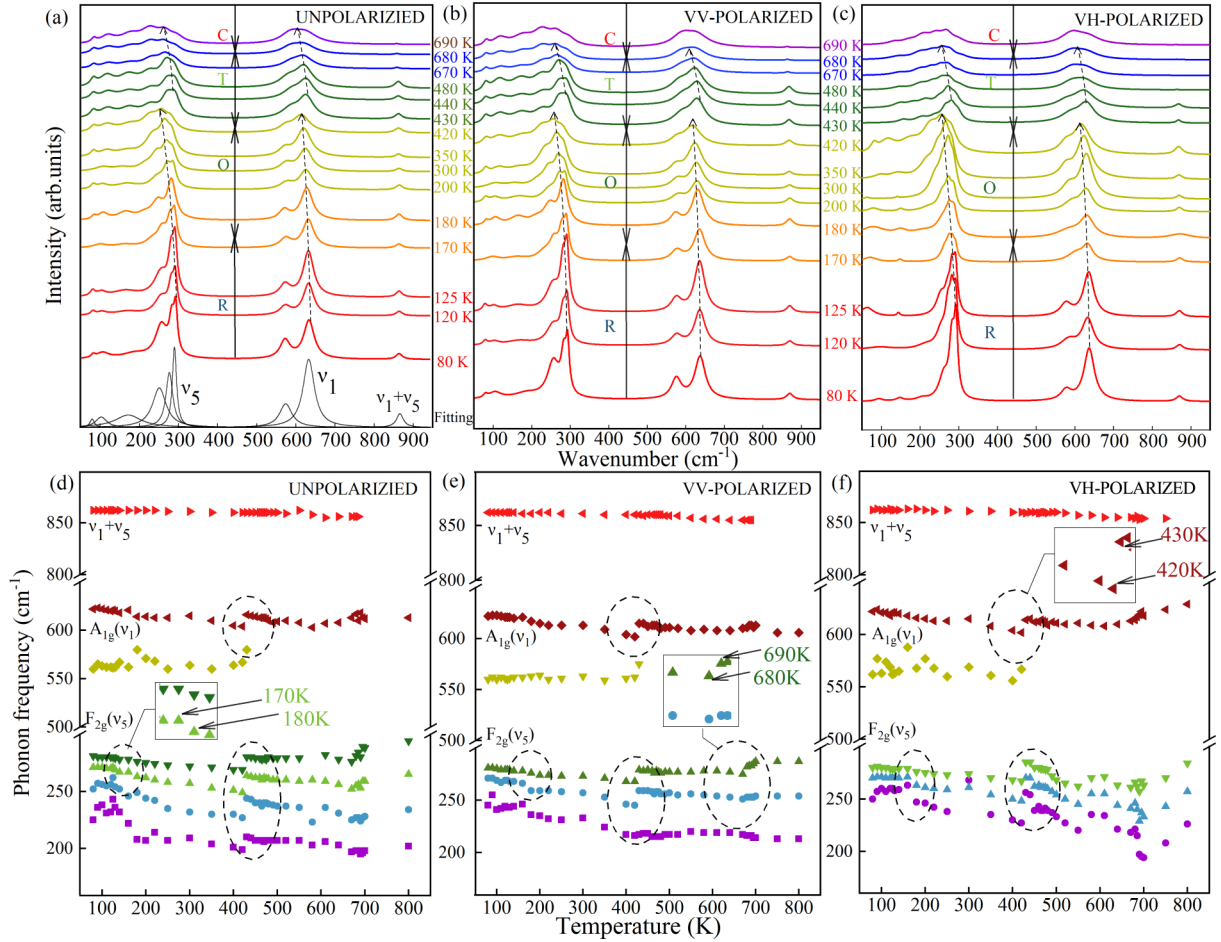
FIG. 3. (a) Unpolarized Raman spectra of KNNLB-25Mn single crystal collected at temperature range of 80–700 K. The multi-Lorentz peak fitting with respect to the vibration modes of lattice at 80 K is shown at the bottom. (b) and (c) Parallel-polarized (VV) and cross-polarized (VH) Raman spectra of KNNLB-25Mn recorded at 80–700 K, respectively. Temperature dependence of phonon frequency corresponding to the main vibration modes of KNNLB extracted from (d) unpolarized, (e) parallel-polarized, and (f) cross-polarized scattering configurations, respectively. The dashed ellipses highlight the abnormal shift of frequency.

determine the lattice structure by investigating an anomaly in frequency shift under the control of an external factor, such as stress and temperature. In heat field, an abnormal shift of frequency could be used to easily judge phase transition after eliminating the thermal effect on lattice. Unpolarized and polarized (VV and VH modes) Raman spectroscopic diagrams of KNNLB-25Mn collected at different temperatures are plotted in Figs. 3(a)–3(c). The peaks below 200 cm^{-1} are overwhelmingly derived from the motions of the alkaline cations and little behaviors of BO$_6$ rotations. Vibrational peaks from BO$_6$ octahedra mainly present at the wave number ranges of 200–300 and 500–700 cm^{-1} associated with $F_{2g}(\nu_5)$ mode and $A_{1g}(\nu_1)$ and $E_g(\nu_2)$ modes, respectively, with a weak peak at about 860 cm^{-1} from the anharmonic coupling mode of $\nu_1 + \nu_5$, respectively. Temperature dependent frequency is particularly studied in characteristic phonon modes of ν_1, ν_5, $\nu_1 + \nu_5$, which reflects the important details of lattice structure of BO$_6$ octahedra in KNNLB crystals. Frequency of the whole vibrations except for $\nu_1 + \nu_5$ mode obviously shifts to lower value with increasing the temperature. This common rule of redshift with temperature originates from the anharmonic effect, which can be simply expressed by [48,49]

$\omega(T) = \omega_0 + \Delta\omega_E + \Delta\omega_A$, where ω_0 is the extrapolated frequency at 0 K, and $\Delta\omega_A$ represents the pure temperature effect of phonon-phonon coupling. Pure volume effect $\Delta\omega_E$ from thermal expansion reflects that phonon frequency is negatively correlated to temperature. In theory, the decrease of optical phonon energy contributes to the redshift of the phonon frequency from the thermal expansion of lattice. As depicted in the inset of Figs. 3(d)–3(f), phonon frequency shows a skip decline at the temperature range of 170–180 K differing from the thermal-induced regular redshift. After excluding the contributions of lattice expansion and phonon couplings, this abnormal skip shift for phonon frequency below 300 cm^{-1} could be attributed to the R to O phase transition process at a low-temperature range of 170–180 K, while modes of over 500 cm^{-1} see no remarkable change in frequency. Therefore, we claim that phonon modes below 300 cm^{-1} from KNNLB lattice perform more sensitively than those at higher wave number ranges during the R-O phase transition.

In addition, with the heating process, the next anomalous shift in temperature dependent frequency associating with the O-T ordering phase transition occurs at 420–430 K. The dashed ellipses in Figs. 3(d)–3(f) exhibit that almost all
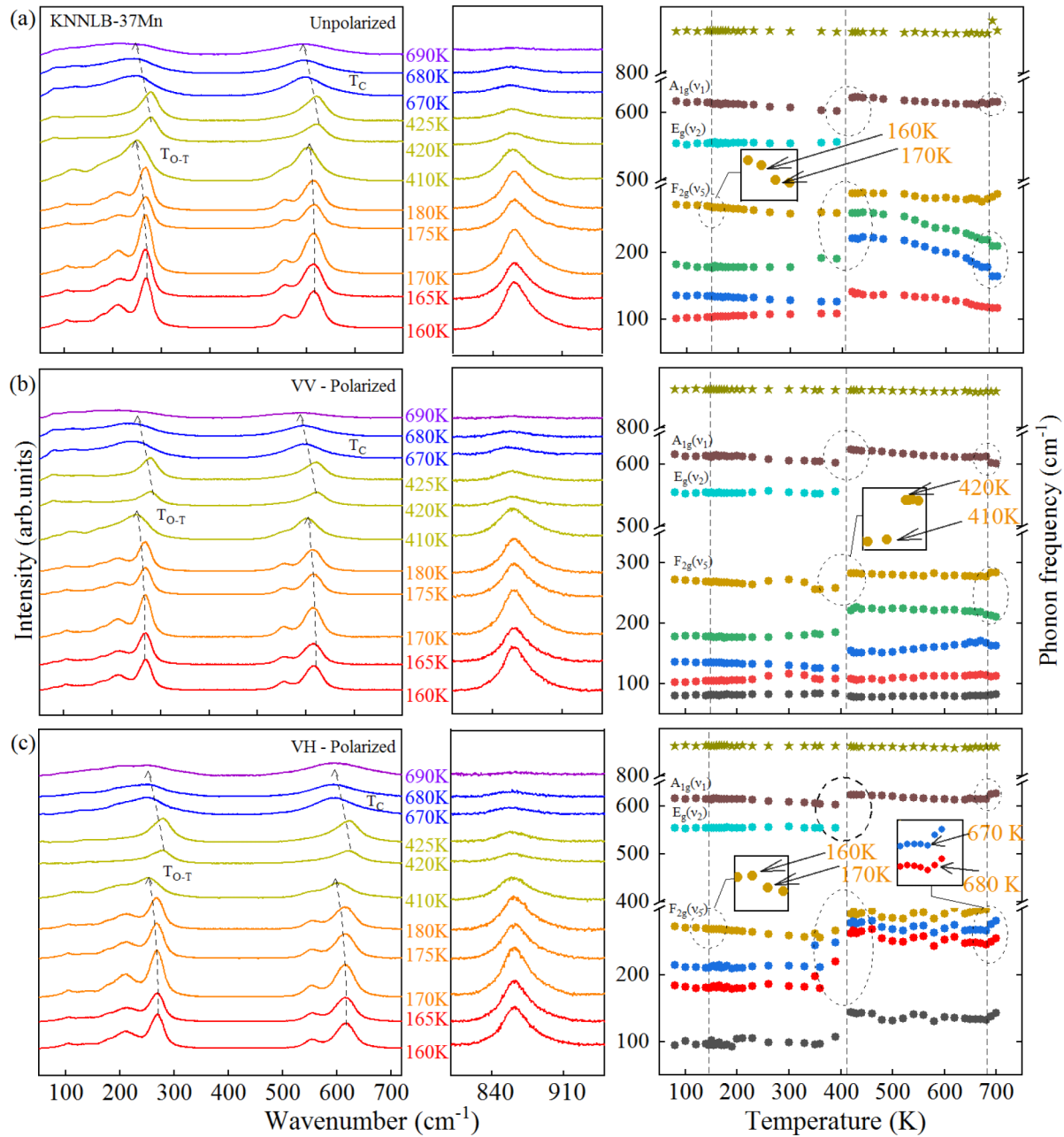
FIG. 4. (a) Unpolarized, (b) parallel-polarized, and (c) cross-polarized Raman spectra of KNNLB-37Mn crystal at the increasing temperature from 80 to 700 K. Spectra at the wave number range of 800–1000 cm^{-1} are enlarged at the middle. The right panels show the temperature dependent phonon frequency of the main vibration modes. The insets and the dashed ellipses highlight the anomalies in frequency evolution.

modes suddenly shift towards higher frequency at this temperature range. The vibration of $E_g(\nu_2)$ mode vanishes at a temperature of over 420 K. Hence, the abnormal blueshift and phonon disappearance could be clear signs for recognizing O-T phase transition. The determination of phase transitions from observing frequency shifts and phonon dynamics is in accordance with the results reported on a KNN-based ferroelectric system [8].

Furthermore, the highly symmetric lattice in higher temperature range would lead to the broadening of scattering peaks. It is mentioned that an isolated peak corresponding to the $\nu_1 + \nu_5$ mode at near 860 cm^{-1} almost annihilates in VH-polarized scattering configuration and greatly reduces in

intensity in unpolarized and VV-polarized geometries with the increasing temperature over 680 K. The gradual overlap of peaks at frequency of below 300 cm^{-1} and 500–700 cm^{-1} makes it difficult to be distinguished. Contrarily, the mode of $\nu_1 + \nu_5$ holds with temperature and then almost vanishes in C phase. Hence, it could determine the Curie temperature (T_c) of 680 K. In terms of T-C phase transition, random and abnormal shift of phonon frequency can also be observed on several main vibrational modes. Therefore, an entire-sequence structural phase transition from R to high-symmetric C phase has been demonstrated during a heating process at 80–800 K.

Similarly, Fig. 4 illustrates temperature dependent Raman spectra on a KNNLB-37Mn single crystal with an increasing

TABLE I. Center frequency collected from unpolarized, VV-polarized, and VH-polarized scattering geometries and depolarization ratio (ρ_l) for R, O, T, and C phases of the main vibrational modes from KNNLB-25Mn and KNNLB-37Mn single crystals. Note that the error bar is estimated by evaluating the contribution of temperature dependent lattice expansion and high reliability of the fitting parameters.

KNNLB-25Mn		ν_5	ν_2	ν_1	$\nu_1 + \nu_5$
R phase	VV (cm^{-1})	282 ± 5.0	576 ± 3.0	632.5 ± 4.5	869.5 ± 0.5
$R3m$	VH (cm^{-1})	288 ± 3.5	583 ± 13.5	631.5 ± 3.5	869.5 ± 0.5
<170 K	Unpolarized (cm^{-1})	278 ± 2.5	563.5 ± 2.5	620.5 ± 2.5	868 ± 1.0
	ρ_l	0.58 ± 0.03	0.51 ± 0.03	0.62 ± 0.03	0.52 ± 0.03
O phase	VV (cm^{-1})	285 ± 5.0	583.5 ± 8.5	629.5 ± 1.0	869 ± 1.0
$Amm2$	VH (cm^{-1})	289.5 ± 7.5	580 ± 9.0	625 ± 3.0	868.5 ± 0.5
170–420 K	Unpolarized (cm^{-1})	275 ± 5.0	570 ± 8.0	615 ± 5.0	868 ± 1.0
	ρ_l	0.68 ± 0.05	0.69 ± 0.02	0.78 ± 0.04	0.54 ± 0.04
T phase	VV (cm^{-1})	289 ± 4.0	586 ± 4.0	624.5 ± 1.5	868.5 ± 0.5
$P4mm$	VH (cm^{-1})	289 ± 9.5	584 ± 7.0	622.5 ± 5.5	869 ± 1.0
420–680 K	Unpolarized (cm^{-1})	278 ± 4.0	–	618 ± 8.0	869 ± 1.0
	ρ_l	0.48 ± 0.04	–	0.51 ± 0.04	0.35 ± 0.02
C phase	VV (cm^{-1})	299 ± 4.0	–	628.5 ± 5.0	868 ± 1.0
$Pm\bar{3}m$	VH (cm^{-1})	289 ± 3.0	–	621.5 ± 3.5	869 ± 1.0
>680 K	Unpolarized (cm^{-1})	284 ± 4.0	–	613.5 ± 3.5	869 ± 1.0
	ρ_l	0.30 ± 0.02	–	0.28 ± 0.01	0.30 ± 0.01
KNNLB-37Mn		ν_5	ν_2	ν_1	$\nu_1 + \nu_5$
R phase	VV (cm^{-1})	269.5 ± 2.5	553 ± 1.0	613.5 ± 2.5	862.5 ± 0.5
$R3m$	VH (cm^{-1})	268.5 ± 2.5	553 ± 1.0	613.5 ± 2.5	862.5 ± 2.5
<160 K	Unpolarized (cm^{-1})	268.5 ± 2.5	553.5 ± 1.5	613.5 ± 2.5	862.5 ± 0.5
	ρ_l	0.55 ± 0.03	0.52 ± 0.04	0.42 ± 0.03	0.53 ± 0.03
O phase	VV (cm^{-1})	274 ± 8.0	554 ± 2.5	613 ± 11.0	862.5 ± 0.5
$Amm2$	VH (cm^{-1})	261 ± 6.0	553.5 ± 2.5	610.5 ± 7.5	861.5 ± 0.5
160–410 K	Unpolarized (cm^{-1})	273.5 ± 14.5	551.5 ± 2.5	607 ± 6.0	861.5 ± 0.5
	ρ_l	0.69 ± 0.05	0.72 ± 0.02	0.7 ± 0.04	0.74 ± 0.04
T phase	VV (cm^{-1})	279.5 ± 2.5	–	616.5 ± 5.5	859.5 ± 1.5
$P4mm$	VH (cm^{-1})	285.5 ± 4.0	–	610.5 ± 7.5	858.5 ± 1.5
410–670 K	Unpolarized (cm^{-1})	282.5 ± 2.5	–	608 ± 8.0	856 ± 1.0
	ρ_l	0.58 ± 0.04	–	0.61 ± 0.04	0.62 ± 0.02
C phase	VV (cm^{-1})	280 ± 4.0	–	606 ± 6.0	859 ± 0.5
$Pm\bar{3}m$	VH (cm^{-1})	291 ± 6.0	–	603 ± 3.0	859 ± 1.0
>670 K	Unpolarized (cm^{-1})	298 ± 6.0	–	598 ± 2.0	859 ± 1.0
	ρ_l	0.26 ± 0.02	–	0.28 ± 0.01	0.31 ± 0.01

Mn content in three varied scattering configurations. According to the careful examination of phonon thermodynamics, R-O phase transition could be found at a temperature of 160–170 K, as shown in the inset enlarging a drastic shift distinguished from the normal thermal-induced shift at 80–160 K. Then, when the temperature rises from 410 to 420 K, O to T phase transformation corresponds to an obvious blueshift of phonon frequency observed from both the ν_1 and ν_5 modes. Both ν_1 and ν_5 modes move toward higher frequency from 410 to 420 K, and a new peak appears at near 50 cm^{-1} in the unpolarized and VV-polarized scattering geometries. Besides, note that peak position of $\nu_1 + \nu_5$ at about 860 cm^{-1} is stable in the heating process. It could be attributed to the apparent vibration of the equatorial oxygen ions in the Nb-O plane and this mode is not sensitive to the temperature [50]. However, the spectra at 830–900 cm^{-1} (see the middle of Fig. 4) indicate clearly that the peak of $\nu_1 + \nu_5$ vibration almost disappears when the temperature reaches over 680 K. Combining with

the similar anomalies of frequency evolution from other main phonon modes, this phenomenon near the range of 670–680 K would be ascribed to T-C phase transition with spontaneous polarization fading away at 680 K.

Therefore, a full ordering structure transformation (R-O-T-C) of KNNLB-37Mn crystal could be determined by studying details of temperature dependent frequency for the core vibrations of BO$_6$ octahedra. In order to specify details of the core phonon modes from BO$_6$ octahedra of KNNLB crystals in each phase, we list the entire phonon frequency in Table I derived by the unpolarized and polarized scattering geometries. As we know, phonon frequency as well as the linewidth (or called full width of half maximum, FWHM) is related and highly sensitive to the molecular structure and phase transition.

In Fig. 5 FWHM values of $A_{1g}(\nu_1)$, $A_{1g}(\nu_1)$, and $\nu_1 + \nu_5$ modes on both KNNLB-25Mn and KNNLB-37Mn are also investigated at the temperature ranging from 80 to 700 K.
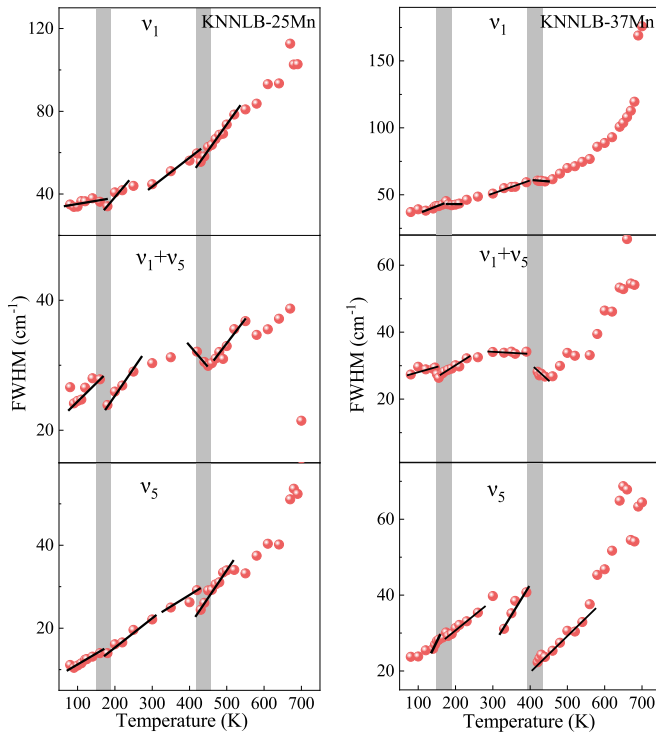
FIG. 5. Temperature dependent FWHM for the $A_{1g}(\nu_1)$, $F_{2g}(\nu_5)$, and $\nu_1 + \nu_5$ modes from KNNLB-25Mn and KNNLB-37Mn crystals. The solid lines are linear fittings with a temperature range near the phase transition point marked as the shaded area.

FIG. 6. Temperature dependent normalized intensity of polarized scattering from KNNLB-37Mn corresponding to the ν_1 and ν_5 modes. The dashed lines and arrows point out the location of phase transition.

It is found that the thermal evolution of FWHM keeps increasing during the heating process. The anharmonic effect in the lattice system would lead to the broadening of phonon vibrational modes and make the harmonic normal phonon interact with each other. Temperature dependence of FWHM can be described as $\Gamma = \Gamma_0 + \eta[1 + e^{-m} + e^{-n}]$, where $m = \hbar\omega_1/2k_BT$, $n = \hbar\omega_2/2k_BT$, Γ_0 is the broadening of the phonon modes originating from the disorder of the lattice, which is irrelevant to the temperature [51], η represents the broadening of phonon modes due to phonon decay, ω_1 and ω_2 follow the restriction of keeping the sum of $\omega_1 + \omega_2 = \omega$, and ω is the wave number of phonon modes. It is worth noting that the FWHM value follows a monotonic relationship within a phase and associates with obvious changes of slope at the region of phase transition. As illustrated in Fig. 5, the slope presents distinct deviations in the shaded area for both doping contents. When the temperature crosses 160 and 170 K for R to O transition of KNNLB-25Mn and KNNLB-37Mn, respectively, the FWHM evolutions are again well described by temperature induced anharmonic effect until the next transition of O-T appears at 420 and 430 K, respectively. When the temperature exceeds 430 K, the FWHM follows the normal thermal induced anharmonic shift. It means that there are two anharmonicities accompanying R-O and O-T phase transition, indicating the phase transforming into another symmetry with the transitional areas revealing the phase coexistence. With the heating process, ferroelectric-paraelectric T-C phase transition would be difficult to be precisely recognized by reading FWHM evolution due to the gradual broadening of all peaks. However, phonon frequency and FWHM fail to quantify the
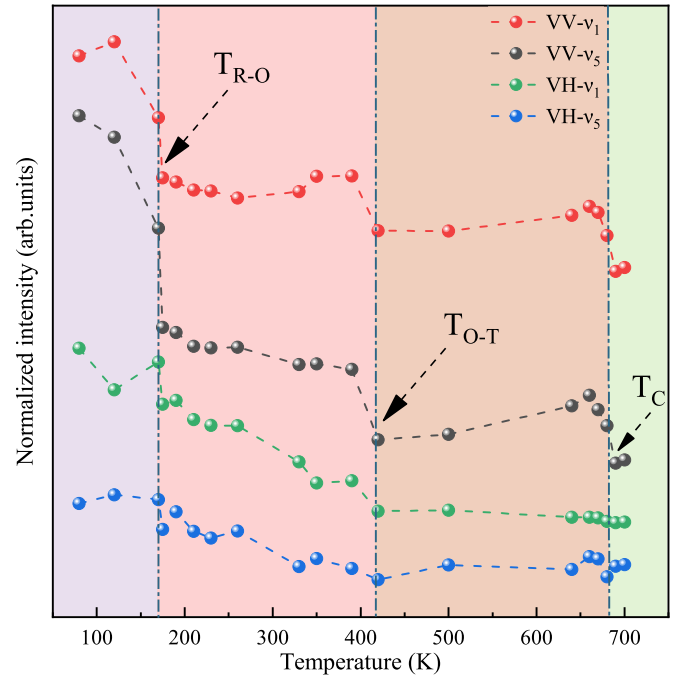
details of phase structure and analyze the characteristic parameters like lattice symmetry, spontaneous polarization of ferroelectrics, order of phase transition, and so on.

Particularly, the polarized scattering intensity has been proven to illustrate the molecular symmetry and the order of phase transition by evaluating evolution of the phonon characteristics. Our previous paper [26] has reported that the polarized scattering intensity is proportional to the polarizability. Thus, it confirms that the polarized scattering intensity would be sensitive to the structural change with phase transition. Figure 6 shows the temperature dependence of normalized intensity in the parallel- and cross-polarized scattering geometries from KNNLB-37Mn. With the temperature increases, the polarized scattering intensities of both VV and VH modes would gradually decrease, but with some sudden drop at near 160, 410, and 680 K. Sharp reduction in intensity directly indicates the discontinuous dynamics of molecular polarizability of KNNLB. Lattice polarizability collected by evaluating the polarized scattering intensity indicates the discontinuity of phase transition. In other words, it confirms that a complete phase transition ordering of R-O-T-C all belongs to the first-order discontinuous transition in KNNLB crystals.

Key characteristics in a first-order phase transition are the phase coexistence and thermal hysteresis, which are observed before [20,52]. Additionally, anomalies of the polarized scattering intensity are associated with the symmetry breaking and symmetry rearrangement during phase transition. Whenever the phase transition belongs to first order or second order, symmetry evolution of lattice has to be discontinuous, owing to the definite symmetry elements in each structure.
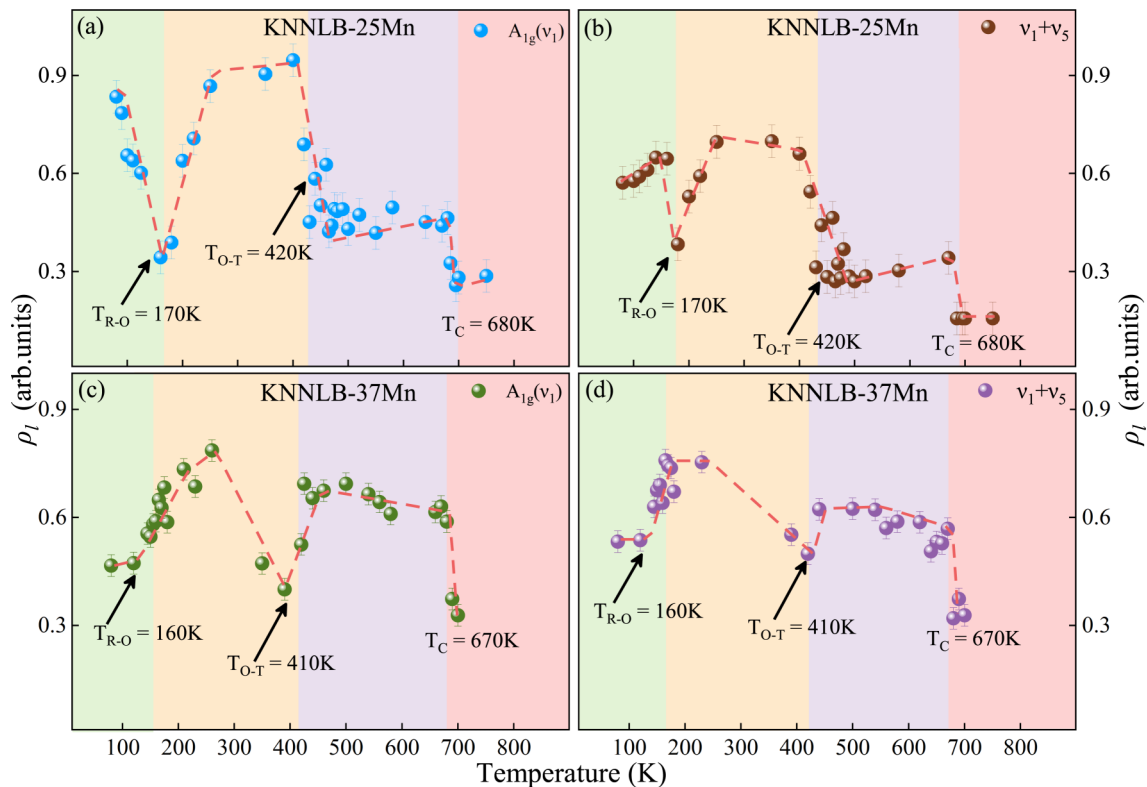
FIG. 7. Temperature dependence of depolarization ratio from (a) and (b) KNNLB-25Mn and (c) and (d) KNNLB-37Mn single crystals in regard to ν_1 and $\nu_1 + \nu_5$ modes.

Polarized scattering performs its superiority on determining the dependence of molecular symmetry under the external fields. The intensity ratio of VH-mode to VV-mode scattering, named as depolarization ratio, could powerfully reflect temperature dependence of symmetry on the random-oriented scatterers or the oriented crystals [53–55]. Depolarization ratio (ρ_l) can be calculated by $\rho_l = \frac{I_{VH}}{I_{VV}}$. In terms of ABO$_3$-type perovskite ferroelectrics, such as Pb(Zn,Nb)O$_3$-PbTiO$_3$ and (Na,Bi)TiO$_3$-BaTiO$_3$ [28,33], depolarization ratio would be competent for dissecting molecular vibration behavior and recognizing phonon configurations. In Fig. 7 the depolarization ratio (ρ_l) of ν_1 and $\nu_1 + \nu_5$ modes of two crystals is plotted. Specifically, Table I lists the details of depolarization ratio associating with the frequency of main vibration modes from BO$_6$ octahedra in each phase of KNNLB-25Mn and KNNLB-37Mn. Figures 7(b) and 7(d) illustrate temperature dependence of ρ_l value for the mode of $\nu_1 + \nu_5$, corresponding to three transition regions of KNNLB-25Mn and KNNLB-37Mn. For KNNLB-25Mn, there are three plunge changes at the temperatures of 170, 420, and 680 K, corresponding to three phase transitions region and symmetry arrangement processes, respectively. In comparison, temperatures of symmetry breaking on KNNLB-37Mn are around 160, 410, and 670 K. It clearly shows that the structural transition point for the heavier doping of KNNLB goes down around 10 K. For the temperature over 680 K, highly symmetric lattice resulting in the value of ρ_l sharply decreased corresponding to the cubic phase. The evolution of the depolarization ratio reflects the structure transformation and reveals the evolution of lattice symmetry in a full phase diagram.

Moreover, the ρ_l value tending to be zero ($\rho_l = 0$) reflects a spherical-like symmetric structure, while an increasing value of ρ_l means that the molecule is evolving to the linear symmetric one [53,55]. For T phase of KNNLB-37Mn, ρ_l values associating with main phonon of ν_1, ν_5 and $\nu_1 + \nu_5$ modes are about 0.58 ± 0.04, 0.61 ± 0.04, and 0.62 ± 0.02, while those of KNNLB-25Mn at T phase are 0.48 ± 0.04, 0.51 ± 0.04, and 0.35 ± 0.02. Obviously, larger ρ_l value for KNNLB single crystal with higher Mn doping content can be observed. It implies that the increasing content of Mn element will stretch the molecule to the linear-oriented vibrational configuration, by comparing values of T phase from Table I and Fig. 7. As we know, the cubic phase ($T > T_c$) holds the lattice parameter of $a = b = c$, while T phase ($T_{O-T} < T < T_c$) of perovskite lattice would present the relationship of $a = b < c$. For T phase of KNNLB perovskite, a bigger value of c/a ratio of the unit cell is generally associated with the increasing extent of the stretched tetragonal molecule geometry [24]. Consequently, results of depolarization ratio demonstrate that the increasing Mn content would not only distort the lattice structure, but also strengthen the tetragonality.

Raman spectroscopic experiments with the deep investigation of phonon characteristics under the temperature field have systematically revealed a complete diagram of first-order phase transition in Mn doping KNNLB single crystals. Simultaneously, through dissecting the temperature dependent linewidth of unpolarized and polarized scattering configurations, we confirm that there is multiphase coexistence near the transition boundary, which greatly contributes to the enhancement of piezoelectric and dielectric properties of lead-free

KNN-based ferroelectrics. In general, ferroelectric spontaneous polarization (P_s) is regarded as the order parameter for discussing the phase transition, according to the crystalline system energy following the relationship of Gibbs free-energy. In the KNN system, its first-order transition process would be associated with the discontinuity of structure properties, such as P_s ordering evolution, atomic rearrangement, and symmetry breaking at the phase boundary of R-O, O-T, and T-C processes. One of the effective approaches to explore the discontinuity of phase transformation in KNN-based crystal is piezoresponse force microscopy (PFM), which is based on scanning probe microscopic technique. Our previous report has revealed the discontinuous evolution during O-T and T-C phase transition of P_s as out-of-plane and in-plane domain pattern by PFM on a Li-doping KNN crystal under a thermal cycle [20]. In this work, temperature dependent intensity of the VV- or VH-mode polarized scattering has enabled us to be sensitive and proportional to the molecular polarizability, which could be defined as $\alpha_{ij} = \Sigma\alpha_a + \Sigma\alpha_b$. α_a is the atomic polarizability explaining the atomic displacement polarization, while α_b is the bond polarizability corresponding to the chemical bond property. Therefore, if the evolution of the order parameter P_s is discontinuous during the first-order phase transitions in KNN lattice, polarizability α_{ij} will also correspond to a same change following discontinuous evolution. The present results of depolarization ratio with respect to temperature $\rho_l(T)$ in Fig. 7 also confirm our conclusion, further figuring out the discontinuity in thermally induced transformation of ferroelectric BO_6 octahedral polarization during the complete R-O, O-T, and T-C phase transition processes.

Moreover, Mn doping might be useful to improve the functionalities of KNN-based crystals, such as low leakage current, electromechanical response, polarization, ferroelectric, and dielectric properties, as specifically demonstrated in Fig. 1. According to the experimental results of x-ray photoelectron spectroscopy (XPS) on KNNLB-37Mn single crystal [17], the asymmetric peaks located at around 639.8 and 652.0 eV correspond to Mn $2p_{3/2}$ and Mn $2p_{1/2}$ peaks, which could assign Mn ion in KNNLB lattice to a mixed valence state of +2 and +4. The position of Mn cation in A (Na^+, K^+, Li^+) or B (Nb^{5+}) site could be experimentally decided by the X-band electron spin resonance (ESR) spectroscopy, which has been revealed on Mn-doped niobate-based ferroelectrics, such as KNN [16], $NaNbO_3$ [15], and $KNbO_3$ [56]. In view of the chemical structure, the heterovalent addition of Mn^{2+} at A site is stabilized by the reduction ($Nb^{5+} \rightarrow Nb^{4+}$) of a certain amount of niobium cations. Additionally, Mn ion at B site is considered as a buffering species for suppressing the increased hole by oxidation process in Mn-doped crystals [16]. It leads to the valence transition from Mn^{2+} to Mn^{4+} with absorbing more holes, following $Mn'''_{Nb} + h^{\cdot} \longrightarrow Mn''_{Nb}$ and $Mn''_{Nb} + h^{\cdot} \longrightarrow Mn'_{Nb}$. The d-electron conduction through Nb^{4+} makes high leakage current in KNN based crystal at a reduced state. In other words, the increasing valence of Mn substituting Nb cation associating with the electron-hole absorption during oxidation is the key contribution for reducing the leakage current. Therefore, the Mn cation in the KNNLB single crystal would substitute A or B sites of ABO_3 perovskite structure, depending on double possible electronic

state [15–17,56]. It has further impacts on phase behaviors of KNN. From the analyses of temperature dependent Raman scattering, we indicate that the high concentration of Mn addition would effectively reduce the temperatures of R-O, O-T, and T-C phase transitions. This doping effect on the phase transition point is also observed in agreement with the anomalous peaks of temperature dependent dielectric constant and dielectric loss [Figs. 1(d) and 1(e)]. Additionally, larger piezoresponse of KNNLB-37Mn than that of KNNLB-25Mn reflects that the increasing content of Mn would effectively stabilize phase coexistence near phase boundary, which is another typical characteristics of discontinuous phase transition in KNNLB crystals.

IV. CONCLUSIONS

In this work, environment-friendly, high-quality, and large-size MnO_2-doped KNNLB single crystals are fabricated by the SFSSCG technique and possess the excellent ferroelectric, piezoelectric, and dielectric properties. We systematically study phonon characteristics, first-order phase transition, and molecular symmetry of KNNLB single crystals with different Mn-doping concentrations by evaluating the polarized and unpolarized Raman spectra from 80 to 800 K. A complete phase transition ordering (R-O-T-C) has been judged and accurately depicted by investigating phonon frequency, linewidth, polarized scattering intensity, and depolarization ratio, respectively. This discontinuous and anomalous evolution in phonon frequency and FWHM value marks the transformation of the lattice structure corresponding to the complete phase transition ordering with the phase coexistence. Polarized Raman scattering intensity is proportional to the polarizability and sensitive to the symmetry rearrangement during the structural transformation. Significantly, evolution of the depolarization ratio can directly quantify the vibrational configuration and further reflect the change of molecule symmetry accompanied with phase transition.

The temperatures of the phase transition thoroughly reduce about 10 K in KNNLB-37Mn than those in KNNLB-25Mn, due to the heavier Mn doping leading to the enhanced distortion in BO_6 octahedra. Simultaneously, the calculated value of the depolarization ratio of KNNLB-37Mn lattice at tetragonal phase is bigger than that of KNNLB-25Mn crystal in comparison. It indicates that the increasing content of Mn in the KNNLB system could effectively strengthen the tetragonality, corresponding to an increscent c/a ratio of the ABO_3 cell. We have discussed the key lattice characteristics of lead-free KNN system during the full-ordering phase transitions. It would boost the whole comprehension of structure properties in high-performance KNN crystals, and promote the development and applications of further investigation in field of lead-free ferroelectrics.

[1] Y. Saito, H. Takao, T. Tani, T. Nonoyama, K. Takatori, T. Homma, T. Nagaya, and M. Nakamura, Nature (London) **432**, 84 (2004).

[2] R. Guo, L. E. Cross, S-E. Park, B. Noheda, D. E. Cox, and G. Shirane, Phys. Rev. Lett. **84**, 5423 (2000).

[3] F. Rubio-Marcos, R. López-Juárez, R. Rojas-Hernandez, A. Campo, N. Raze-Pérez, and J. Fernaddez, ACS Appl. Mater. Interfaces **7**, 23080 (2015).

[4] X. Wang, J. Wu, D. Xiao, J. Zhu, X. Cheng, T. Zheng, B. Zhang, X. Lou, and X. Wang, J. Am. Chem. Soc. **136**, 2905 (2014).

[5] J. G. Hao, W. Li, J. W. Zhai, and H. Chen, Mat. Sci. Eng. R **135**, 1 (2019).

[6] K. Wang, F. Z. Yao, W. Jo, D. Gobeljic, V. V. Shvartsman, D. C. Lupascu, J. Li, and J. Rödel, Adv. Funct. Mater. **23**, 4079 (2013).

[7] Y. Yang, Y. Ji, M. Fang, Z. Zhou, L. Zhang, and X. Ren, Phys. Rev. Lett. **123**, 137601 (2019).

[8] J.-F. Li, K. Wang, F.-Y. Zhu, L.-Q. Cheng, and F.-Z. Yao, J. Am. Ceram. Soc. **96**, 3677 (2013).

[9] H. Y. Park, C. W. Ahn, H. C. Song, J. H. Lee, S. Nahm, K. Uchino, and H. Lee, Appl. Phys. Lett. **89**, 062906 (2006).

[10] X. Lv, N. Zhang, J. G. Wu, and X.-X. Zhang, Acta Mater. **197**, 224 (2020)

[11] C. Y. Shi, J. Ma, J. Wu, K. Chen, and B. Wu, Ceram. Int. **46**, 2798 (2020).

[12] S. J. Zhang, R. Xia, T. R. Shrout, G. Z. Zang, and J. F. Wang, J. Appl. Phys. **100**, 104108 (2006).

[13] D. M. Lin, K. W. Kwok, and H. L. W. Chan, J. Appl. Phys. **102**, 034102 (2007).

[14] M. Matsubara, K. Kikuta, and S. Hirano, J. Appl. Phys. **97**, 114105 (2005).

[15] J. Kubacki, A. Molak, and E. Talik, J. Alloys Compd. **328**, 156 (2001).

[16] Y. Kizaki, Y. Noguchi, and M. Miyayama, Appl. Phys. Lett. **89**, 142910 (2006).

[17] M. H. Jiang, J. W. Zhang, G. H. Rao, D. Li, C. A. Randall, T. Li, B. L. Peng, L. Li, Z. F. Gu, X. Y. Liu, and H. T. Huang, J. Mater. Chem. C **7**, 14845 (2019).

[18] T. G. Xu, X. Zhao, and Y. F. Zhu, J. Phys. Chem. B **110**, 25825 (2006).

[19] I. N. Lin, C. T. Chia, H. L. Liu, Y. C. Chen, H. F. Cheng, and C. C. Chi, J. Eur. Ceram. Soc. **23**, 2633 (2003).

[20] A. Y. Cui, K. Jiang, P. Zhang, L. P. Xu, G. S. Xu, X. M. Chen, Z. G. Hu, and J. H. Chu, J. Phys. Chem. C **121**, 14322 (2017).

[21] K. Kakimoto, K. Akao, Y. Guo, and H. Ohsato, Jpn. J. Appl. Phys. **44**, 7064 (2005).

[22] R. Ratheesh, H. Sreemoolanadhan, and M. T. Sebastian, J. Solid State Chem. **131**, 2 (1997).

[23] A. Cui, K. Jiang, M. Jiang, L. Shang, L. Zhu, Z. Hu, G. Xu, and J. Chu, Phys. Rev. Appl. **12**, 054049 (2019).

[24] R. Singh, K. Kambale, A. Kulkarni, and C. Harendranath, Mater. Chem. Phys. **138**, 905 (2013).

[25] Y. Ye, A. Y. Cui, M. Y. Bian, K. Jiang, L. Q. Zhu, J. Z. Zhang, L. Y. Shang, Y. W. Li, Z. G. Hu, and J. H. Chu, Phys. Rev. B **102**, 024103 (2020).

[26] A. Y. Cui, Y. Ye, L. M. Zheng, K. Jiang, L. Q. Zhu, L. Y. Shang, Y. W. Li, Z. G. Hu, and J. H. Chu, Phys. Rev. B **100**, 024102 (2019).

[27] S. Klauer and M. Wöhlecke, Phys. Rev. Lett. **68**, 3212 (1992).

[28] N. Waeselmann, B. Mihailova, B. J. Maier, C. Paulmann, M. Gospodinov, V. Marinova, and U. Bismayer, Phys. Rev. B **83**, 214104 (2011).

[29] W. L. Zhu, J. L. Zhu, M. S. Wang, B. Zhu, X. H. Zhu, and G. Pezzottia, J. Raman Spectrosc. **43**, 1320 (2012).

[30] S. Sanna, S. Neufeld, M. Rüsing, G. Berth, A. Zrenner, and W. G. Schmidt, Phys. Rev. B **91**, 224302 (2015).

[31] S. Tsukada, Y. Fujii, Y. Yoneda, H. Moriwake, A. Konishi, and Y. Akishige, Phys. Rev. B **97**, 024116 (2018).

[32] K. Chen, G. S. Xu, D. F. Yang, and X. F. Wang, J. Appl. Phys. **101**, 044103 (2007).

[33] G. de la Flor, T. Malcherek, S. Gorfman, and B. Mihailova, Phys. Rev. B **96**, 214102 (2017).

[34] A. M. Mazuera, P. S. Silva, Jr., A. D. Rodrigues, P. S. Pizani, Y. Romaguera-Barcelay, M. Venet, and M. Algueró, Phys. Rev. B **94**, 184101 (2016).

[35] M. Bah, F. Giovannelli, R. Retoux, J. Bustillo, E. L. Clezio, and I. Monot-Laffez, Cryst. Growth Des. **16**, 315 (2016).

[36] Y. Liu, G. Xu, J. Liu, D. Yang, and X. Chen, J. Alloys Compd. **603**, 95 (2014).

[37] L. Zheng, X. Huo, R. Wang, J. Wang, W. Jiang, and W. Cao, Cryst. Eng. Commun. **15**, 7718 (2013).

[38] M. H. Jiang, C. A. Randall, H. Z. Guo, G. H. Rao, R. Tu, Z. F. Gu, G. Cheng, X. Y. Liu, J. W. Zhang, and Y. X. Li, J. Am. Ceram. Soc. **98**, 2988 (2015).

[39] J. Zhang, M. H. Jiang, G. Cheng, Z. Gu, X. Liu, J. Song, L. Li, and Y. Du, Ferroelectrics **502**, 210 (2016).

[40] K. Song, Z. Lin, and Z. Xu, Ceram. Int. **41**, S100 (2015).

[41] W.-L. Zhou and Z.-Y. Zhao, Chinese Phys. B **25**, 037102 (2016).

[42] F. Rubio-Marcos, A. Del Campo, R. López-Juárez, J. J. Romero, and J. F. Fernández, J. Mater. Chem. **22**, 9714 (2012).

[43] Y. Inagaki, K.-i. Kakimoto, and I. Kagomiya, J. Am. Ceram. Soc. **93**, 40615 (2010).

[44] A. W. Hewat, J. Phys. C: Solid State Phys. **6**, 2559 (1973).

[45] G. Shirane, H. Danner, A. Pavlovic, and R. Pepinsky, Phys. Rev. **93**, 672 (1954).

[46] V. J. Tennery, J. Am. Ceram. Soc. **48**, 537 (1965).

[47] J.-J. Zhou, J.-F. Li, K. Wang, and X.-W. Zhang, J. Mater. Sci. **46**, 5111 (2011).

[48] S. Najmaei, P. Ajayan, and J. Lou, Nanoscale **5**, 9758 (2013).

[49] X. T. Huang, Y. Gao, T. Q. Yang, W. C. Ren, H. M. Cheng, and T. S. Lai, Sci. Rep. **6**, 32236 (2016).

[50] Q. Q. Li, J. Y. Wang, M. J. Li, S. Guo, J. Z. Zhang, Z. G. Hu, Z. Y. Zhou, G. S. Wang, X. L. Dong, and J. H. Chu, Phys. Rev. B **96**, 024101 (2017).

[51] H. Terrones, F. López-Urías, and M. Terrones, Sci. Rep. **3**, 1549 (2013).

[52] L. P. Xu, K. Jiang, J. Z. Zhang, G. S. Xu, Z. G. Hu, and J. H. Chu, Appl. Phys. Lett. **106**, 122901 (2015).

[53] C. Banwell and E. McCash, *Fundamentals of Molecular Spectroscopy* (McGraw-Hill, New York, 1994).

[54] D. A. Long, *Raman Spectroscopy* (McGraw-Hill, New York, 1977).

[55] W. Hayes and R. Loudon, *Scattering of Light by Crystals* (John Wiley & Sons, New York, 1978).

[56] K. Kakimoto, I. Masuda, and H. Ohsato, Jpn. J. Appl. Phys. Part 1 **43**, 6706 (2004).